Journal for ImmunoTherapy of Cancer

Single-cell RNA-sequencing atlas reveals an FABP1-dependent immunosuppressive environment in hepatocellular carcinoma

Weiwei Tang ,[1] Guangshun Sun,[2] Gu-Wei Ji ,[1] Tingting Feng,[3] Qian Zhang,[1] Hengsong Cao,[2] Wenhao Wu,[2] Xiaoyi Zhang,[2] Chuan Liu,[1] Hanyuan Liu,[2] Tian Huang,[1] Li Liu,[4] Yongxiang Xia ,[1] Xuehao Wang[1]

To cite: Tang W, Sun G, Ji G-W, *et al*. Single-cell RNA-sequencing atlas reveals an FABP1-dependent immunosuppressive environment in hepatocellular carcinoma. *Journal for ImmunoTherapy of Cancer* 2023;**11**:e007030. doi:10.1136/jitc-2023-007030

► Additional supplemental material is published online only. To view, please visit the journal online (http://dx.doi.org/10.1136/jitc-2023-007030).

WT, GS, G-WJ and TF are joint first authors.

Accepted 31 October 2023

For numbered affiliations see end of article.

Correspondence to
Dr Xuehao Wang; wangxh@njmu.edu.cn

Dr Yongxiang Xia; yx_xia@njmu.edu.cn

Dr Li Liu; jewtou@gmail.com

ABSTRACT

Background Single-cell RNA sequencing, also known as scRNA-seq, is a method profiling cell populations on an individual cell basis. It is particularly useful for more deeply understanding cell behavior in a complicated tumor microenvironment. Although several previous studies have examined scRNA-seq for hepatocellular carcinoma (HCC) tissues, no one has tested and analyzed HCC with different stages.

Methods In this investigation, immune cells isolated from surrounding normal tissues and cancer tissues from 3 II-stage and 4 III-stage HCC cases were subjected to deep scRNA-seq. The analysis included 15 samples. We distinguished developmentally relevant trajectories, unique immune cell subtypes, and enriched pathways regarding differential genes. Western blot and co-immunoprecipitation were performed to demonstrate the interaction between fatty acid binding protein 1 (FABP1) and peroxisome proliferator-activated receptor gamma(PPARG). In vivo experiments were performed in a C57BL/6 mouse model of HCC established via subcutaneous injection.

Results FABP1 was discovered to be overexpressed in tumor-associated macrophages (TAMs) with III-stage HCC tissues compared with II-stage HCC tissues. This finding was fully supported by immunofluorescence detection in significant amounts of HCC human samples. FABP1 deficiency in TAMs inhibited HCC progression in vitro. Mechanistically, FABP1 interacted with PPARG/CD36 in TAMs to increase fatty acid oxidation in HCC. When compared with C57BL/6 mice of the wild type, tumors in FABP1–/– mice consistently showed attenuation. The FABP1–/– group's relative proportion of regulatory T cells and natural killer cells showed a downward trend, while dendritic cells, M1 macrophages, and B cells showed an upward trend, according to the results of mass cytometry. In further clinical translation, we found that orlistat significantly inhibited FABP1 activity, while the combination of anti-programmed cell death 1(PD-1) could synergistically treat HCC progression. Liposomes loaded with orlistat and connected with IR780 probe could further enhance the therapeutic effect of orlistat and visualize drug metabolism in vivo.

Conclusions ScRNA-seq atlas revealed an FABP1-dependent immunosuppressive environment in HCC. Orlistat significantly inhibited FABP1 activity, while the combination of anti-PD-1 could synergistically treat HCC progression. This study identified new treatment targets and strategies for HCC progression, contributing to patients with advanced HCC from new perspectives.

WHAT IS ALREADY KNOWN ON THIS TOPIC

⇒ Although several previous studies have examined single-cell RNA sequencing (scRNA-seq) for hepatocellular carcinoma (HCC) tissues, no one has tested and analyzed HCC with different stages.

WHAT THIS STUDY ADDS

⇒ Fatty acid binding protein 1 (FABP1) was overexpressed in tumor-associated macrophages (TAMs) with III-stage HCC tissues relative to II-stage HCC tissues, and such conclusion was fully confirmed by immunofluorescence detection in large HCC human samples. Inhibition of FABP1 in TAMs restricted HCC progression in vitro and in vivo. Moreover, FABP1 interacted with peroxisome proliferator-activated receptor gamma(PPARG) in TAMs to promote fatty acid oxidation and progress of HCC. We found in further clinical practice that orlistat significantly inhibited FABP1 activity, while the combination of anti-programmed cell death 1(PD-1) could synergistically treat HCC progression. Liposomes loaded with orlistat and connected with IR780 probe could further enhance the therapeutic effect of orlistat and visualize drug metabolism in vivo.

HOW THIS STUDY MIGHT AFFECT RESEARCH, PRACTICE OR POLICY

⇒ Our scRNA-seq atlas revealed an FABP1-dependent immunosuppressive environment in HCC. This study identified new treatment targets and strategies for HCC progression, contributing to patients with advanced HCC from new perspectives.

INTRODUCTION

Hepatocellular carcinoma (HCC) is a prevalent primary liver cancer, which occupies

about 90% of all liver cancer cases.[1] HCC ranks fifth among all common cancers worldwide and the third greatest cause of death related to cancer, according to the WHO.[2] The rate of HCC varies between geographic regions. It is more prevalent in undeveloped regions of the world; for instance, its yearly incidence rate exceeds 15 per 100,000 people in East Asia and sub-Saharan Africa. However, HCC incidence is rising quickly in Europe and the USA and is predicted to do so for the next 10 years.[3 4]

Different staging systems, such as tumor-node-metastasis (TNM), Okuda, the Cancer of the Liver Italian Program, Japan Integrated Staging, and Barcelona Clinic Liver Cancer, serve for the prediction of patients with HCC's survival.[5 6] Using a TNM classification, the American Joint Committee on Cancer/International Union Against Cancer staging approach conducts a stratification on patients with HCC, which takes tumor size and quantity, vascular invasion, bilobar involvement, and extrahepatic metastasis into account, and a high TNM stage implies a bad prognosis for patients with HCC. However, the molecular mechanism behind the progression of low-TNM to high-TNM-stage HCC malignancies remains unknown. Consequently, it is of critical importance to elucidate the pathogenesis of HCC progression and to identify predictors and treating targets.

Single-cell RNA sequencing (scRNA-seq) emerges as a new technique for analyzing single-cell cells. scRNA-seq becomes more sensitive, accurate and efficient with the development of single-cell isolation techniques with strong sensitivity, automaticity and low cost, and the improvement of high-throughput technologies and enhanced operational procedures. ScRNA-seq helps to understand cell biological behavior more deeply in a complex tumor cell, particularly by analyzing the single-cell populations.[7–9] The process that cancer cells enter and alter the architecture of the surrounding tissue is accompanied by the generation of the tumor microenvironment (TME). TME is a unique ecosystem comprised of tumor, immune, and stromal cells that provides a safe niche for tumor cells to grow.[10] In TME, the oxygen concentration is low, metabolite accumulation changes, pH value reports acidic, and there are immunosuppressive cytokines and growth hormones, which constitute its common abiotic characteristics. Not only do these harsh conditions affect the repertoire of tumor cells, but they also have a profound effect on the function and health regarding resident cell populations and those infiltrated by tumors. The TME stimulates regulatory immune cell differentiation, restricts immune cell activation, and triggers cell death or prevents immune cell growth.[11] In the present investigation, deep scRNA-seq was carried out on immune cells isolated in cancer tissues and adjacent representative tissues from 3 II-stage and 4 III-stage HCC cases including a total of 15 samples. For the purpose of obtaining the overall spectra of cancer cell compositions, classification was conducted on one subdivided cell in the isolating process of CD45, for ensuring the process regarding numerous immune-related cells. We identified various immune cell subtypes, including macrophage, natural killer (NK), B lymphocyte, CD8+T lymphocyte, and CD4+T lymphocyte, as well as relevant developmental and enrichment mechanisms. Interestingly, fatty acid binding protein 1 (FABP1) was found overexpressed in tumor-associated macrophages (TAMs) with III-stage HCC tissues compared with II-stage HCC tissues, and immunofluorescence detection in more HCC human samples validated this conclusion. In this study, FABP1 function and mechanism in TAMs of HCC were also elaborated in detail.

RESULTS

ScRNA-seq profile acquisition of samples and data generation in II and III stage HCC samples

For analyzing immune cells related to HCC progression, deep scRNA-seq was conducted on immune cells isolated from cancer tissues and adjacent representative tissues of 3 II-stage and 4 III-stage HCC cases. The analysis process included 15 samples (figure 1A). For capturing the overall composition regarding cancer cells, we conducted the sorting of one subdivided cell in the isolating process of CD45, to analyze the process regarding different immunity-related cells. The Uniform Manifold Approximation and Projection(UMAP) plot showed that the identification and merger process of markers were considered to name five respective immune cell clusters (figure 1B–D, online supplemental figure S1A). For example, T/NK cell cluster mainly expressed CD3B, CD3E, CD8A, FOXP3, CTLA4, *etc*. Mono/Mac cell cluster mainly expressed CD14, S100A8, CD68, CD163, *etc*. Mast cell cluster mainly expressed TPSAB1, TPBS2, CPA3 (figure 1C–D, online supplemental figure S1A). As shown in figure 1E, UMAP showed the distribution of individual cell populations in various types of tissue samples including Tumor (II), Tumor (III), Normal (II), Normal (III), Thrombus (III), Microvascular invasion (MVI) (III). Accordingly, the ratio of T/NK in tumor tissues to that in neighboring tissues was lower, while the ratios of Mono/Mac and B/Plasma were higher than that in adjacent tissues. T/NK was significantly lower in MVI and thrombus than it was in tumor tissues. When compared with Tumor (II), the level of T/NK expression in Tumor (III) was significantly lower, whereas the results for Mono/Mac were the complete reverse (figure 1F, online supplemental figure S1B–F). These results not only offered abundant data for a full knowledge of the progression of HCC, but also illustrated in a methodical manner the cell population distribution in the many types of tissues that were studied.

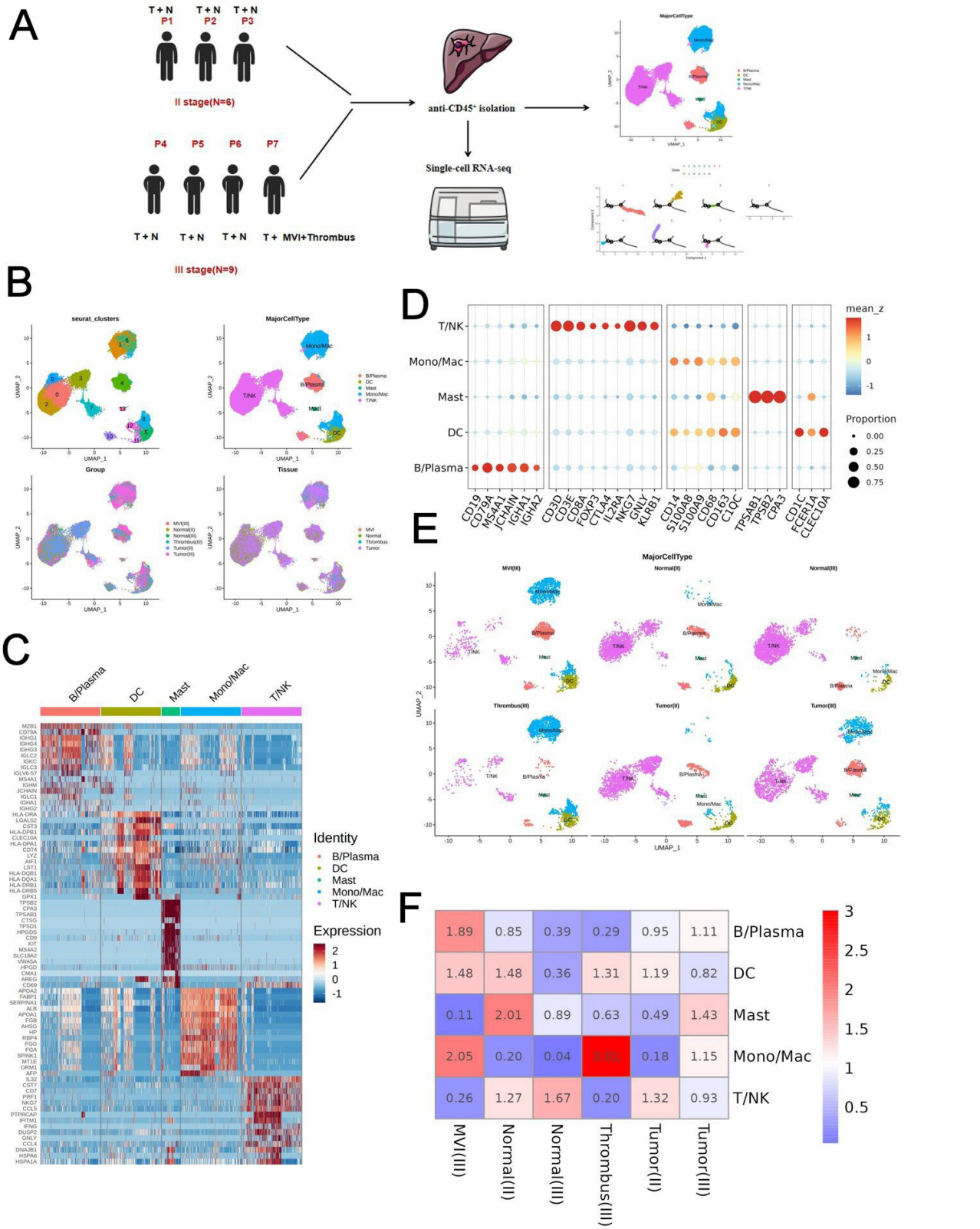

Figure 1 Acquiring scRNA-seq profiles of the samples and generating data in HCC. (A) scRNA-seq on immune cells under the isolation in cancer tissues and adjacent representative tissues of 3 II-stage and 4 III-stage HCC cases, and a total of 15 samples were included in the analysis. (B) UMAP displaying diverse immune cell types which have been discovered. (C) Heat maps displaying different cell populations and the markers that distinguish them. (D) Dot plots illustrating the markers that are unique to each cell population. (E) UMAP displaying the distinct immune cell populations present in the different samples. (F) The bar chart illustrating the variations in expression of the different cell populations present in the different samples including Tumor (II), Tumor (III), Normal (II), Normal (III), Thrombus (III), Microvascular invasion (MVI) (III). UMAP, Uniform Manifold Approximation and Projection; DC, dendritic cells; HCC, hepatocellular carcinoma; NK, natural killer; scRNA-seq, single-cell RNA sequencing.

Analysis of T and NK cell clusters in II and III stage HCC samples

Considering the big role played by T and NK cells in cancer development, we began by conducting an in-depth study on the enrichment and function of various T and NK cell populations found in different HCC stage samples. One CD4 cell cluster (CD4-FOXP3), six CD8 cell clusters (CD8-PDCD1, CD8-BAG3, CD8-TOP2A, CD8-IL-7R, CD8-CCL3L1, CD8-FABP1), and two NK cell clusters (NK-FCGR3A, NK-KLRC1) were given names based on the identification of the markers (figure 2A–D). We conducted enrichment analysis on each subgroup to define its main functions (online supplemental figures S2–10). For example, CD8-PDCD1 was enriched in the programmed cell death 1(PD-1) checkpoint pathway in cancer, which is related to CD8 T-cell exhaustion. CD8-BAG3 was enriched in T-cell activation. Figure 2E demonstrated the degree to which the expression profiles of the various cell groups were comparable to one another. We found that CD4-FOXP3 was the highest expressed in Thrombus and Tumors, CD8-PDCD1 cells were the highest expressed in Tumor tissue, CD8-BAG3 was expressed mainly in Normal and Tumor tissues, CD8-TOP2A and CD8-CCL3L1 were the highest expressed in MVI compared with other tissues, and CD8-FABP1 was the highest expressed in Thrombus, CD8-IL-7R presented a higher expression in II-stage tumor tissues compared with III-stage tumor tissues (figure 2F–G, online supplemental figure S11). Two NK cell populations both presented high expressions in Normal tissues, which were higher in II-stage relative to III-stage tissues (figure 2F,G, online supplemental figure S11). In general, different groups of NK cells and T cells may play different functions in cancer tissues, MVI and tumor thrombus.

Myeloid cell cluster classification and trajectory in II and III stage HCC samples

In this study, we looked in great detail at the many cell clusters that make up myeloid cell. According to the marker identification and merging, the UMAP plot showed that there were four cell clusters that were named Mono-CD14, Mac-COL4A1, Mac-C1QC, and Mac-FABP1 (figure 3A–D). As found, Mac-FABP1 presented a higher expression in Tumor tissues relative to Normal tissues, and that it was also greatly concentrated in MVI and Thrombus. Even more intriguing is the fact that Mac-FABP1 showed an obviously higher expression in III-stage tissues relative to II-stage tissues. The other three subgroups (Mono-CD14, Mac-COL4A1, Mac-C1QC) were highly enriched in normal tissue (figure 3E–G, online supplemental figure S12A). To further understand the differentiation of different myeloid cell populations, trajectory analysis was performed using CytoTRACE. Results showed that Mac-FABP1 was mainly located at the end of myeloid cell development, while Mac-C1QC and Mono-CD14 were located at the early stage of development (figure 4A,B). Tumors (III), MVI, and Thrombus were at the late stages of progression, whereas Tumors (II) and normal tissues were at the early stages, consistent with cancer progression (figure 4C,D). Detailed cluster and locus analysis of myeloid cells provided a theoretical basis for us to search for targets that promote HCC progression.

FABP1 exhibited overexpression in TAMs of III stage HCC tissues compared with II stage tissues

According to the results of the scRNA-seq, Mac-FABP1 may critically impact the TAMs of HCC. As a result, we performed a comprehensive analysis of FABP1 expression in each sample and cell cluster. In the total cell cluster analysis, FABP1 was shown to be considerably abundant in Mac-FABP1, while it was less expressed in dendritic cell (DC) and B/Plasma cells (figure 4E). An analysis of the differences between the samples showed the remarkably higher FABP1 expression in Tumor, MVI, and Thrombus tissues relative to adjacent cancer tissues (figure 4F, online supplemental figure S12B). Fascinatingly, FABP1 presented a higher expression in III-stage cancers relative to II-stage tumors (figure 4g, online supplemental figure S12C). Immunofluorescence testing was analyzed on a total of 27 samples, derived from 15 patients at varying stages of the disease (online supplemental table S1), for the purpose of further validating the results of scRNA-seq. We were taken aback by the discovery that the level of FABP1 expression in the HCC cancer tissues of patients with III-stage cancer was noticeably higher relative to patients with I–II stage cancer. In addition to this, FABP1 exhibited an obviously higher expression in Tumor and MVI relative to Normal tissues (figure 5A, online supplemental figure S12D). These results piqued our interest, which led us to examine FABP1 activity in HCC-derived TAMs.

FABP1 deficiency in TAMs restricted HCC development in vitro

We used TAM supernatant to stimulate HCC cells for more deeply verifying the role of FABP1 in TAMs from HCC in vitro. We found that the expression of FABP1 was significantly increased in TAMs compared with M0 macrophages, indicating that tumor-derived soluble factors might be responsible for this FABP1 upregulation (online supplemental figure S12C). TAMs in the si-FABP1 group remarkably weakened HCC cells in terms of the proliferation, invasion, and migration in comparison to the si-NC group using the5-ethynyl-2' -deoxyuridine(EdU), transwell, and scratch assays (figure 5B–D). According to the results presented above, inhibiting FABP1 in TAMs has the potential to slow down the evolution of HCC.

Macrophagic FABP1 enhanced TAM protumor polarization in HCC

How exactly does a lower level of FABP1 in TAMs prevent the development of HCC? After stimulating THP-1 cells using HCC cancer cell supernatant and co-culturing with

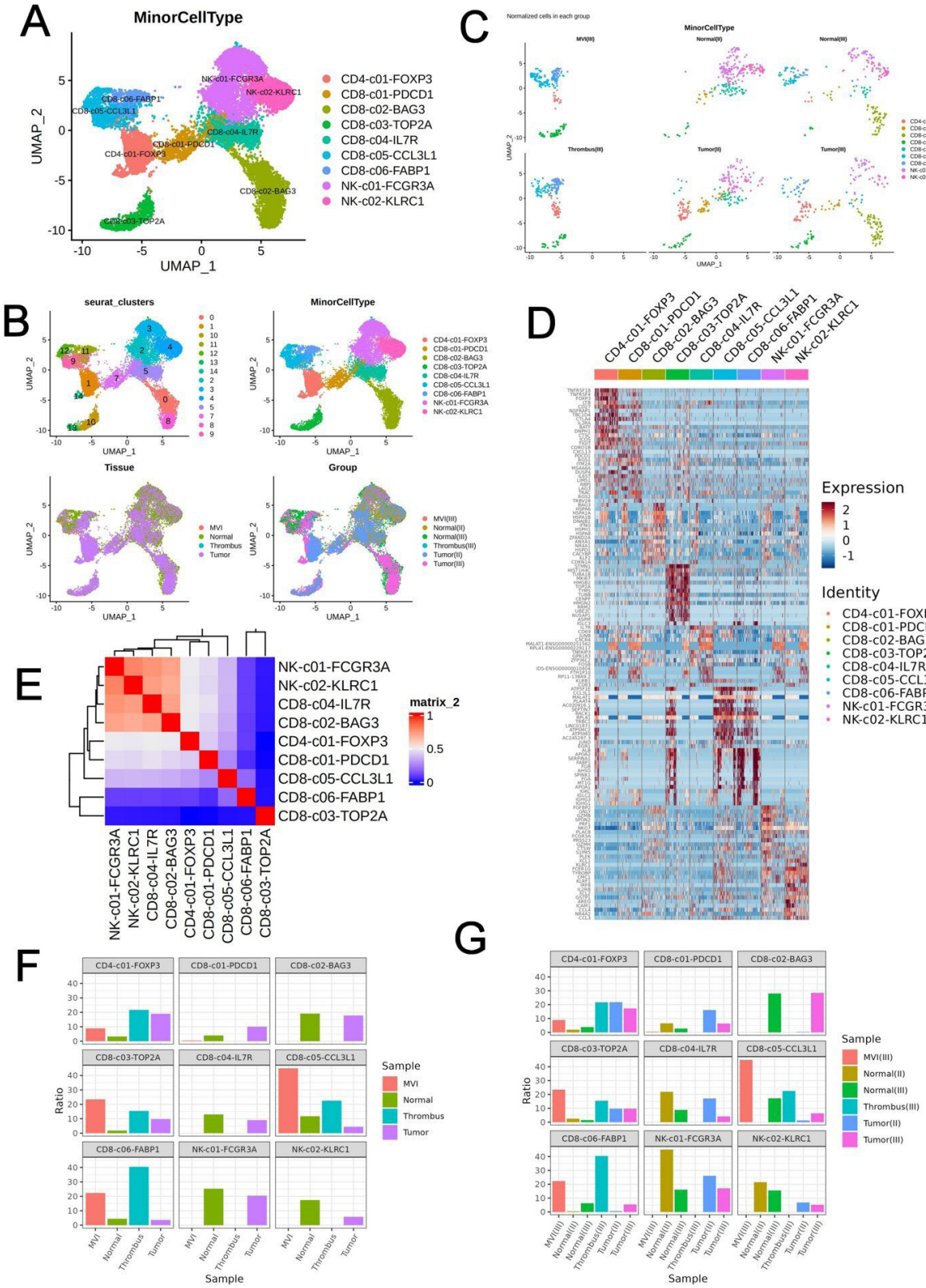

Figure 2 An analysis of T and NK cell clusters in samples from patients with II-stage and III-stage hepatocellular carcinoma. (A) An illustration from UMAP depicting the many T and NK cell types that have been discovered. (B) UMAP displaying distinct T-cell populations and NK cell populations in distinct groups. (C) UMAP demonstrating that various samples contain a variety of T and NK cell populations. (D) Heat maps displaying the many markers that distinguish the T and NK cell populations. (E) Similarity of expression profiles of different cell groups.(F) The bar chart showing T and NK cell population expression in different samples. (G) The bar chart showing T and NK cell population expression in each sample including Tumor (II), Tumor (III), Normal (II), Normal (III), Thrombus (III), Microvascular invasion (MVI) (III). UMAP, Uniform Manifold Approximation and Projection; FABP1, fatty acid binding protein 1; NK, natural killer.

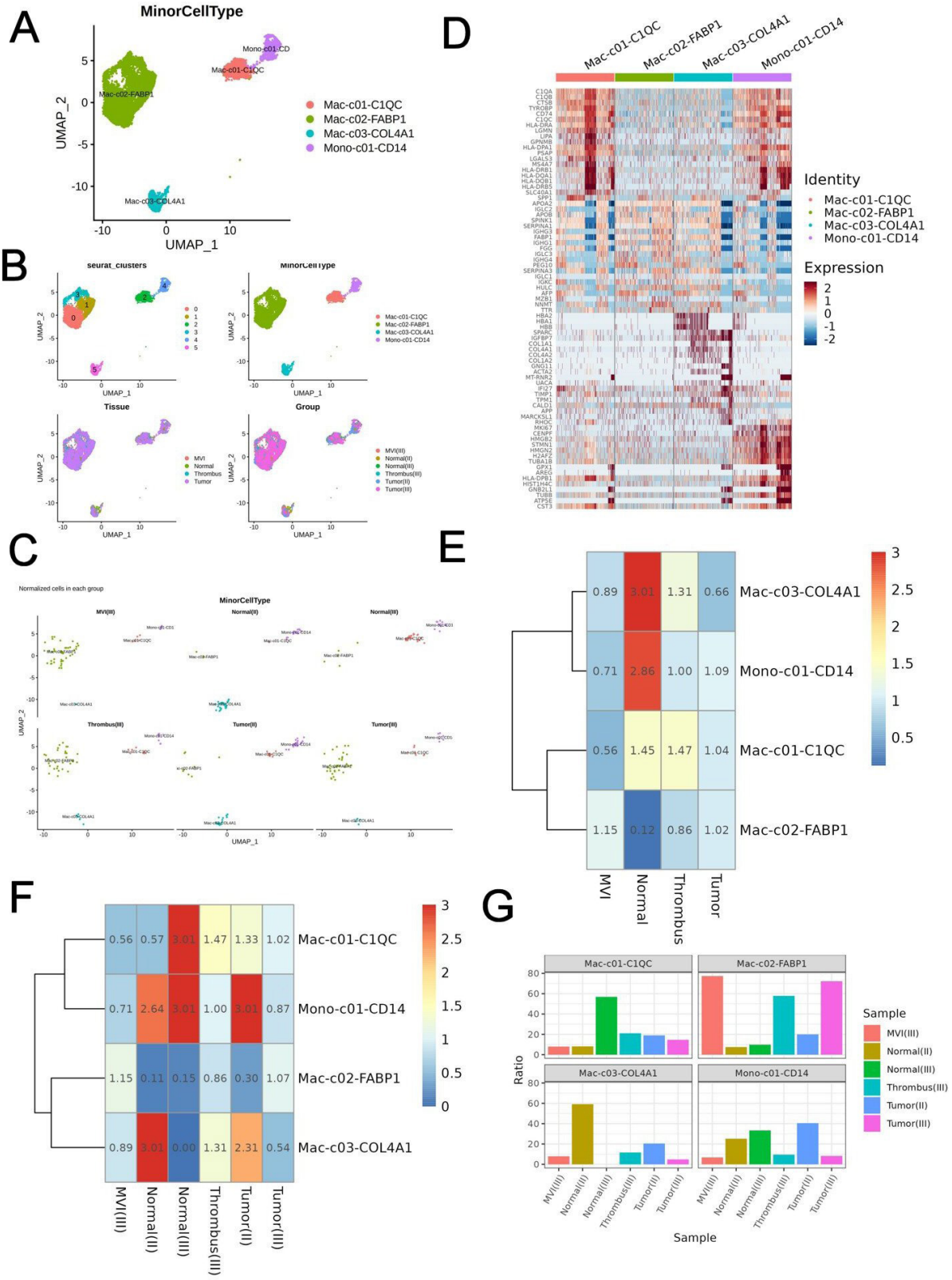

Figure 3 A more in-depth classification of myeloid cell clusters in samples of hepatocellular carcinoma with II-stage and III-stage. (A) An illustration from UMAP illustrating the many myeloid cell populations that have been found. (B) A UMAP displaying the distinct myeloid cell populations separated into their respective groups. (C) UMAP demonstrating the presence of distinct myeloid cell populations in each of the samples. (D) Heat maps displaying the many markers that are unique to each myeloid cell population. (E) The heatmap displaying the expression of the myeloid cell population across the various samples. (F) The heatmap showing myeloid cell population expression in each sample. (G) The bar chart showing myeloid cell population expression in each sample including Tumor (II), Tumor (III), Normal (II), Normal (III), Thrombus (III), Microvascular invasion (MVI) (III). UMAP, Uniform Manifold Approximation and Projection; FABP1, fatty acid binding protein 1.

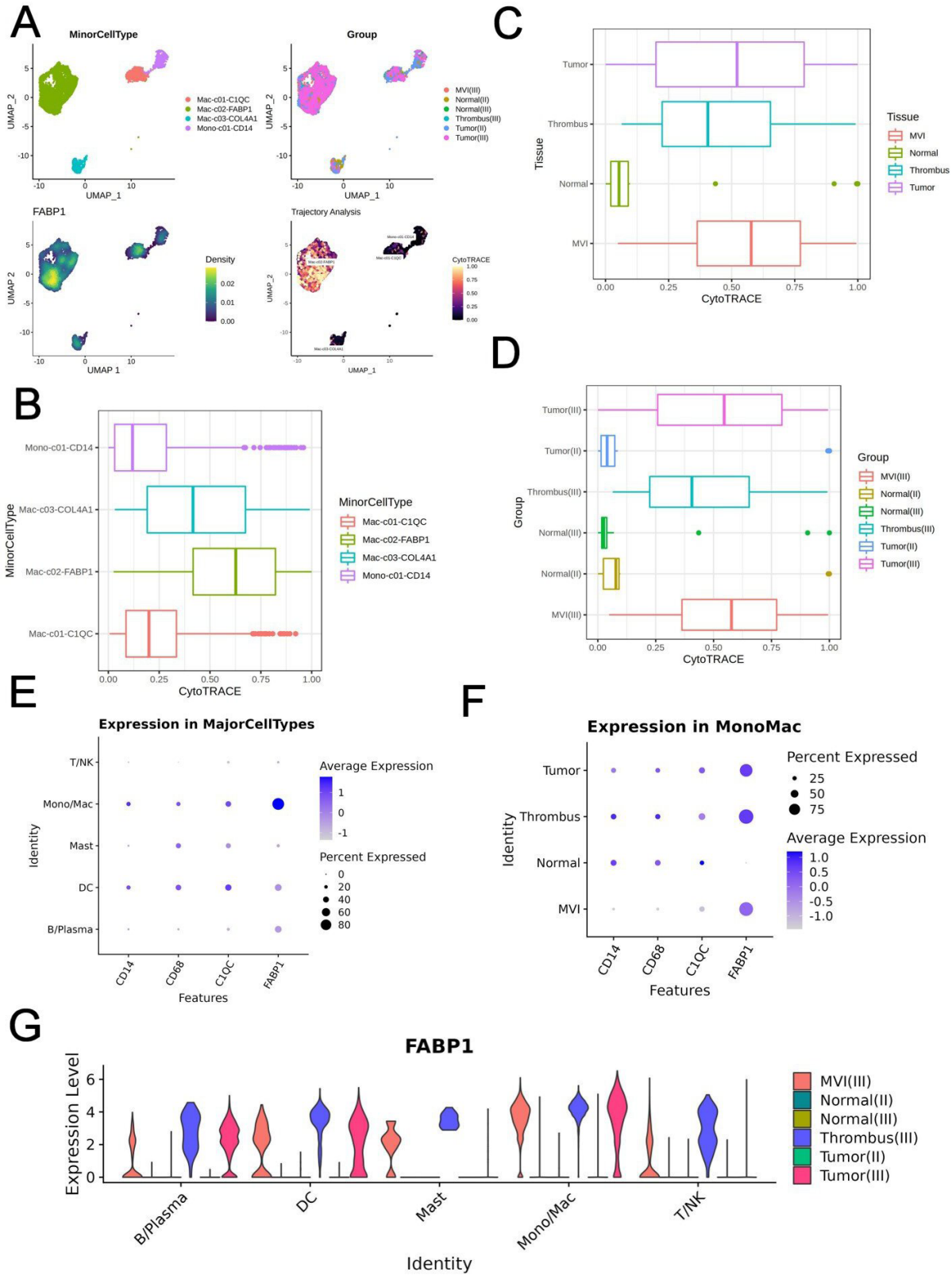

Figure 4 The progression of the myeloid cell cluster distribution over the course of time in the various samples. (A) UMAP illustrating the FABP1 expression in myeloid cell populations. (B) Developmental trajectories of different myeloid subsets by CytoTRACE analysis. (C) Developmental trajectories of different types of samples by CytoTRACE analysis. (D) The developmental trajectory of each tissue sample including Tumor (II), Tumor (III), Normal (II), Normal (III), Thrombus (III), Microvascular invasion (MVI) (III). (E) The dot plots illustrating the expression of FABP1 in the various subsets of data. (F) A dot plot illustrating the expression of FABP1 in a variety of tissue samples. (G) A violin diagram illustrating the expression of FABP1 in various subsets of various tissue samples. UMAP, Uniform Manifold Approximation and Projection; DC, dendritic cell; NK, natural killer; FABP1, fatty acid binding protein 1.

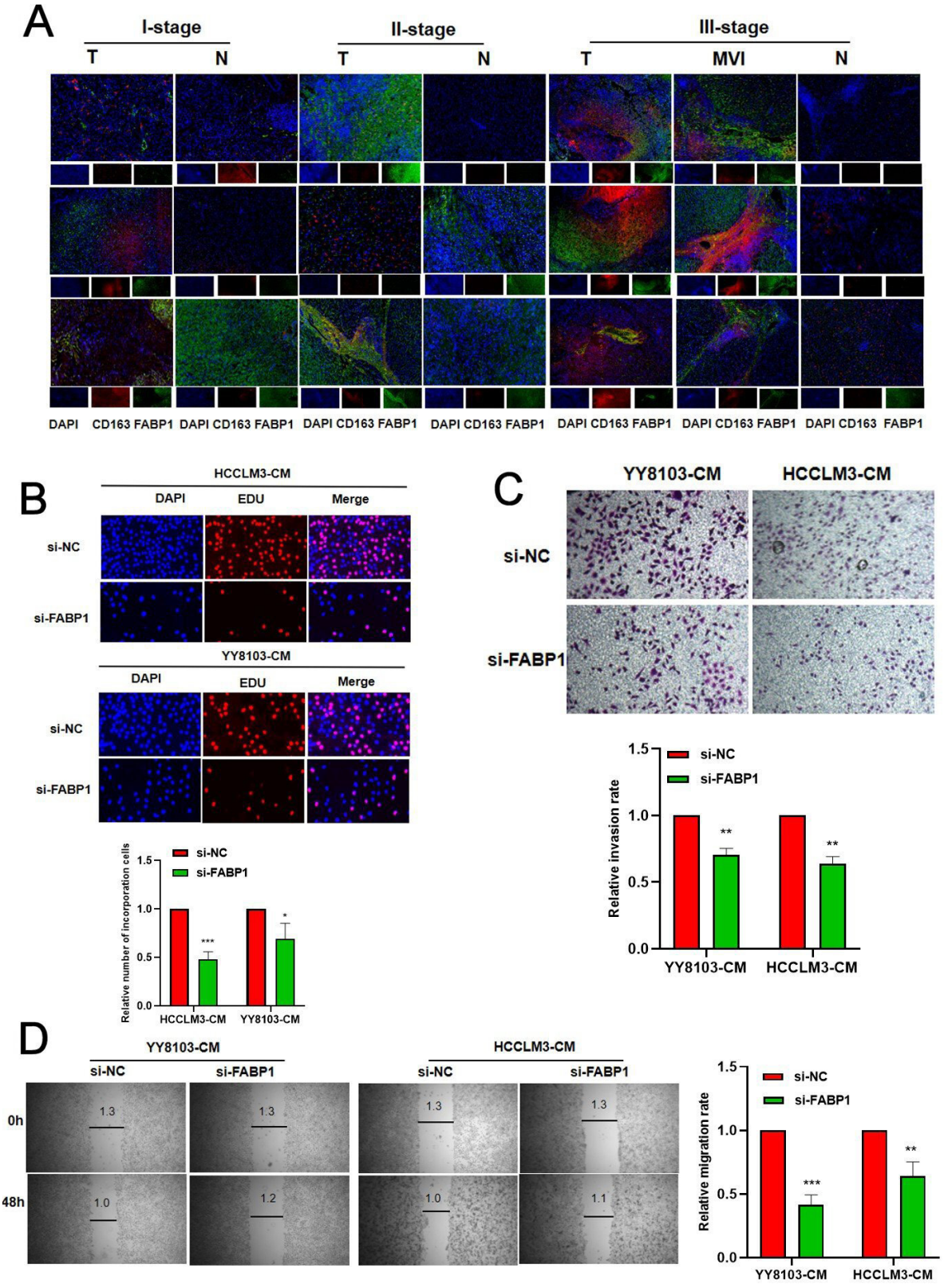

Figure 5 The expression of FABP1 in TAMs of HCC and in vitro confirmation. (A) Immunofluorescence image demonstrating the expression of FABP1 in various tissues taken from patients with HCC at various stages of the disease. A total of 27 samples, derived from 15 patients at varying stages of the disease. Each row represents a patient, and the most representative images of three patients in each stage are displayed here. (B) EdU assay of cancer cells treated with TAM supernatant in various groups. (C) A transwell assay was performed on cancer cells with TAM supernatant using various groups. (D) A scratch assay was performed on cancer cells using TAM supernatant in each of the different groups. *p<0.05, **p<0.01, ***p<0.001. DAPI,4',6-diamidino-2-phenylindole; EdU, 5-ethynyl-2' -deoxyuridine; FABP1, fatty acid binding protein 1; HCC, hepatocellular carcinoma; MVI, Microvascular invasion; TAM, tumor-associated macrophage.

si-NC/si-FABP1, we measured the expression of genes related to TAM using quantitative real time polymerase chain reaction(qRT-PCR). As found, there were obviously higher expressions of CD86, CXCL10, and HLA-DR of the M1 phenotype in the si-FABP1 group relative to the si-NC group. On the other hand, there were lower expressions of CD206 and CD163 of the M2 phenotype relative to the control group (figure 6A,B). It was found that programmed cell death- ligand 1(PD-L1), which is a marker for the M2 phenotype, decreased as well in the si-FABP1 group (figure 6C). According to western blot, the si-FABP1 in TAMs decreased the protein expression level of PD-L1 (figure 6D). Based on these results, it appears that suppressing FABP1 caused TAMs derived from HCC to revert from an M2 phenotype to an M1 phenotype, hence preventing HCC cell proliferation.

FABP1 interacted with PPARG in TAMs to increase fatty acid oxidation in HCC

However, the mechanism by which FABP1 changes the TAM phenotype is a fascinating area of research that warrants additional investigation. It is common knowledge that FABP1 participates in the metabolism process regarding long-chain fatty acid transportation, binding and metabolism.[12–14] We compared the genes and pathways used by the various clusters of myeloid cells and analyzed the results (online supplemental figures S13–17). Mac-FABP1 cell cluster showed that APOA2, APOB, RBP4, *et al* were significantly upregulated while CD74, HLA-DQA1, FCN3, *et al* were downregulated (online supplemental figure S17A). Kyoto Encyclopedia of Genes and Genomes(KEGG) pathway analysis revealed that the several genes that are controlled by Mac-FABP1 are involved in lipid metabolism, the peroxisome proliferator-activated receptor(PPAR) pathway, fat digestion, and other processes (figure 6E). Gene Ontology-biological process(GO-BP) analysis showed that the majority of these genes were enriched in the process of lipid remodeling (figure 6F). Previous study has confirmed that TAMs express scavenger receptor CD36 and accumulate lipids, and obtain energy using fatty acid oxidation (FAO) rather than glycolysis. High level of FAO promotes oxidative phosphorylation of mitochondria leading to regulation of M2 phenotype of TAMs.[15 16] We hypothesize that FABP1 promoted M2 phenotype by activating PPARG/CD36 to regulate FAO. To prove this, the western blot demonstrated decreased PPARG and CD36 expressions in the si-FABP1 group relative to the si-NC group(figure 6G). Co-immunoprecipitation experiments showed that FABP1 and PPAGR communicated with one another and revealed their interaction (figure 6H). In addition to this, the amount of lipid droplets present in the si-FABP1 group was significantly less than what was found in the si-NC group (figure 6I). These results indicate that FABP1 interacts with PPARG to increase FAO and maintain the M2 phenotype of TAMs in HCC.

FABP1 deficiency caused immune activation and strengthened HCC cell sensitivity to anti-PD-1 therapy

Due to the fact that the aforementioned discussions demonstrated the FABP1 mechanism in TAMs, it is important to do additional research on the effect that a lack of FABP1 has on the TME as a whole. The mass cytometry method was used to identify tumor samples of wild-type (WT) mice and FABP1−/− C57BL/6 mice injected with H22 cells, respectively. In total, among the 31 respective cell clusters, each was defined from the others by the respective markers that were characteristic of its constituent cell type (figure 7A,B, online supplemental figure S18). According to the findings, regulatory T cells (Treg), NK and CD8 T cells showed decreased relative proportion in the FABP1−/− (FABP1 knockout) group relative to the WT group. On the other hand, DC, M1 macrophages, and B cells showed an increasing relative proportion (figure 7A–C). However, we found that the ratio of CD8 T cells to all T cells in the WT group was lower than that in the FABP1−/− group (online supplemental figure S19). In addition to this, it was revealed that PD-L1, PD-1, T cell immunoreceptor with Ig and ITIM domains(TIGIT), T cell immunoglobulin and mucin domain-containing protein 3(TIM-3), and Cytotoxic T lymphocyte associate protein-4(CTLA-4) expressions decreased in FABP1−/− deficient mice (figure 7D,E). These results provided further evidence that a lack of FABP1 led to the activation of the immune system in HCC.

In light of the results presented above, we wonder whether the combination of anti-PD-1 and FABP1 knockout can more deeply improve the antitumor effect in the new TME after FABP1 knockout. This is due to the fact that FABP1 knockout reduces the inhibitory TME in HCC. In order to demonstrate the validity of this hypothesis, we first carried out subcutaneous injections of H22 cells into WT and FABP1−/− C57BL/6 mice, and then on day 8, we administered PD-1 monoclonal antibody(mAb) injections to evaluate the mice's ability to fight tumors. At the time of the mice' sacrifice on day 21, it was discovered that FABP1−/− mice had much lower tumor weight and volume relative to WT C57BL/6 mice (figure 8A,B). Relative to the anti-PD-1 group, the FABP1−/− + anti-PD-1 group presented obviously decreased tumor weight and volume (figure 8A,B). According to immunofluorescence, CD86 had a higher expression in the FABP1−/− group relative to the WT group, whereas CD163 showed a lower expression in the FABP1−/− group (figure 8C,D). The deletion of FABP1 caused increased CD8 expression and decreased Ki67, PD-1, and PD-L1 expression, which conformed to mass cytometry results (figure 8E,F). In the FABP1−/− group that received the anti-PD-1 treatment, CD163, PD-1, and PD-L1 expressions decreased even further, whereas the expression of CD86 and CD8 was raised (figure 8C–F).

To further analyze the significance of whether FABP1 participating in the anti-PD-1 therapy resistant in human HCC tissues, we conducted immunofluorescence detection on six puncture samples which were non-responsive

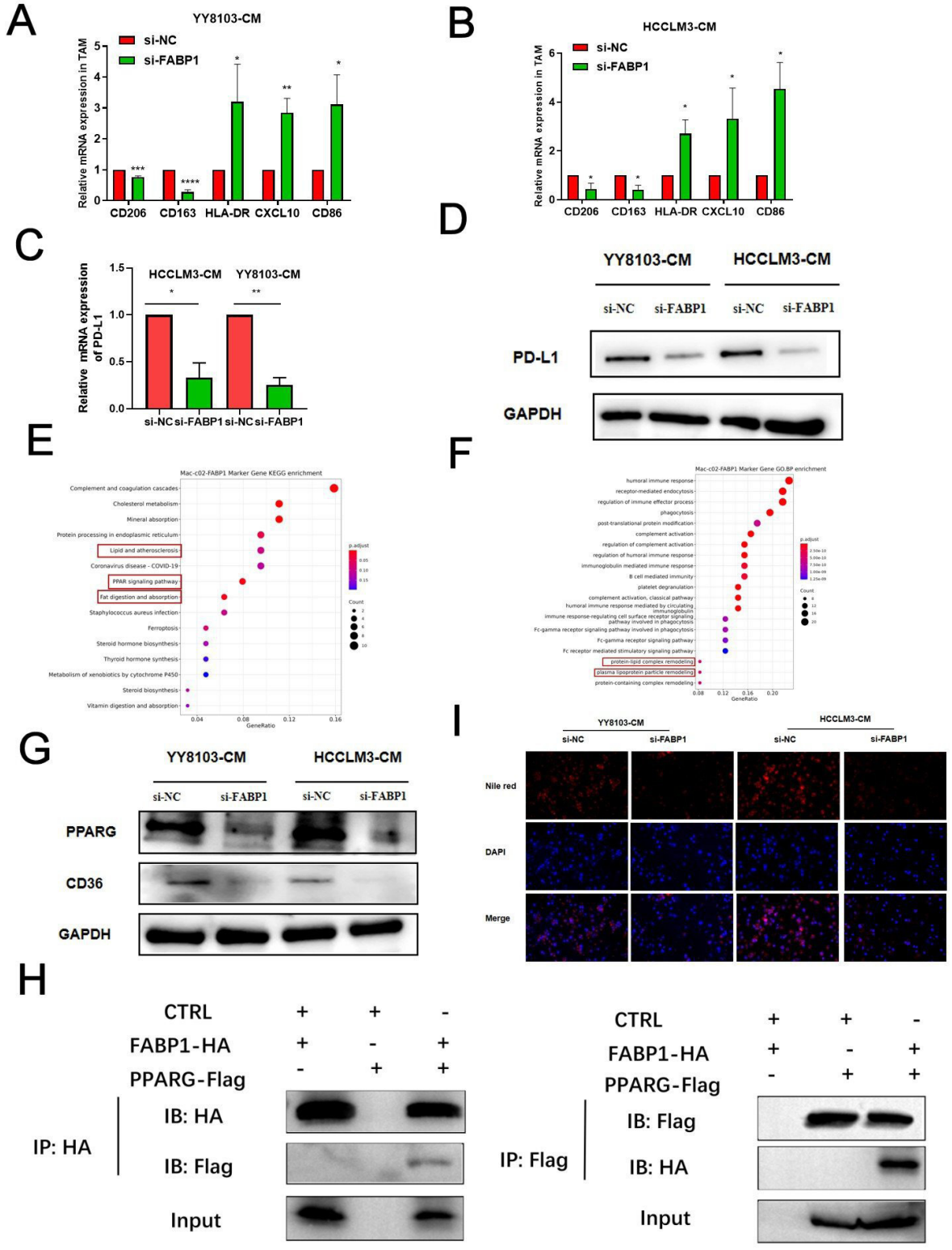

Figure 6 FABP1 interacted with PPARG in TAMs to increase fatty acid oxidation in HCC. (A–B) qRT-PCR results of M1/M2 phenotype gene expression in the si-FABP1 and si-NC group after the addition of HCC cancer cell supernatant to TAM cells activation. (C–D) The expression of PD-L1 messenger RNA and protein that was expressed across the various groups. (E–F) KEGG and GO analysis of differentially expressed genes in the Mac-FABP1 cell cluster. (G) The expression of the proteins PPARG and CD36. (H) Co-immunoprecipitation of FABP1 and PPARG. (I) There is a decrease in the total amount of fat in the si-NC and si-FABP1 groups of TAM cells. *p<0.05, **p<0.01, ***p<0.001,****p<0.0001. qRT-PCR,quantitative real time polymerase chain reaction;PD-L1, programmed cell death- ligand 1;PPARG, peroxisome proliferator-activated receptor gamma;DAPI, 4',6-diamidino-2-phenylindole;GAPDH,glyceraldehyde-3-phosphate dehydrogenase; KEGG, Kyoto Encyclopedia of Genes and Genomes;GO, Gene Ontology;FABP1, fatty acid binding protein 1; HCC, hepatocellular carcinoma; TAM, tumor-associated macrophage.

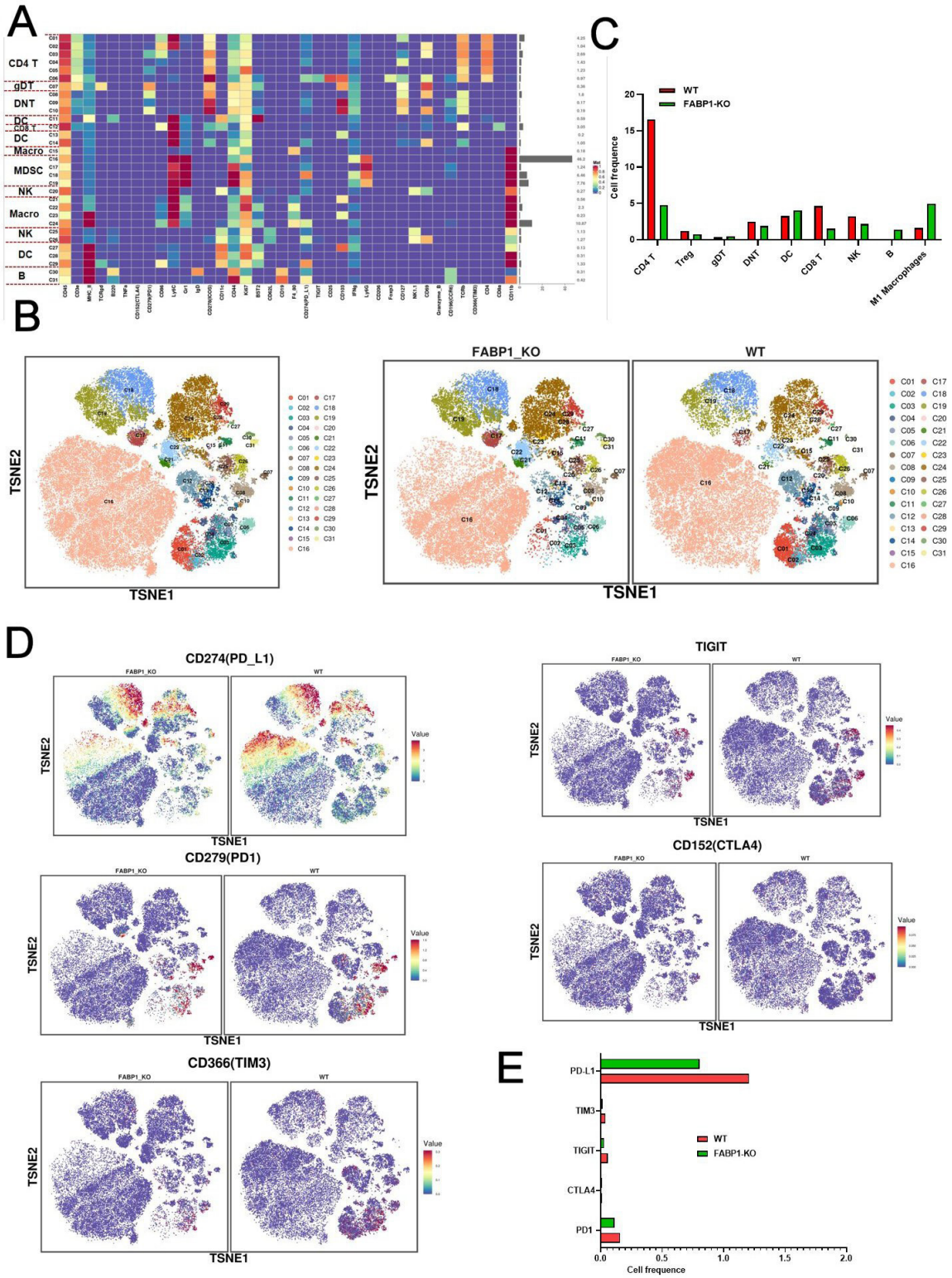

Figure 7 Mass cytometry of tumors from FABP1-KO and WT mice. (A) There were a total of 31 cell clusters that needed to be divided, and each respective cell cluster was subsequently defined. (B) A T-SNE plot illustrating the distribution of 31 cell clusters throughout the respective sample. (C) The histogram that displays the number of instances of each cell cluster across the respective groups. (D) A T-SNE plot illustrating the different groups' distributions of PD-L1, PD-1, TIGIT, TIM-3, and CTLA-4 in subcutaneous hepatocellular carcinoma tumors. (E) A histogram illustrating the distribution of the number of PD-L1, PD-1, TIGIT, TIM-3, and CTLA-4 cells among the various groups. PD-L1,programmed cell death - ligand 1;PD-1, programmed cell death 1; TIGIT,T cell immunoreceptor with Ig and ITIM domains;TIM-3,T cell immunoglobulin and mucin domain-containing protein 3;CTLA-4, Cytotoxic T lymphocyte associate protein-4;MDSC,Myeloid-derived suppressor cells;KO, knockout;T-SNE,t-distributed Stochastic Neighbor Embedding;DC, dendritic cell; FABP1, fatty acid binding protein 1; NK, natural killer; WT, wild type.

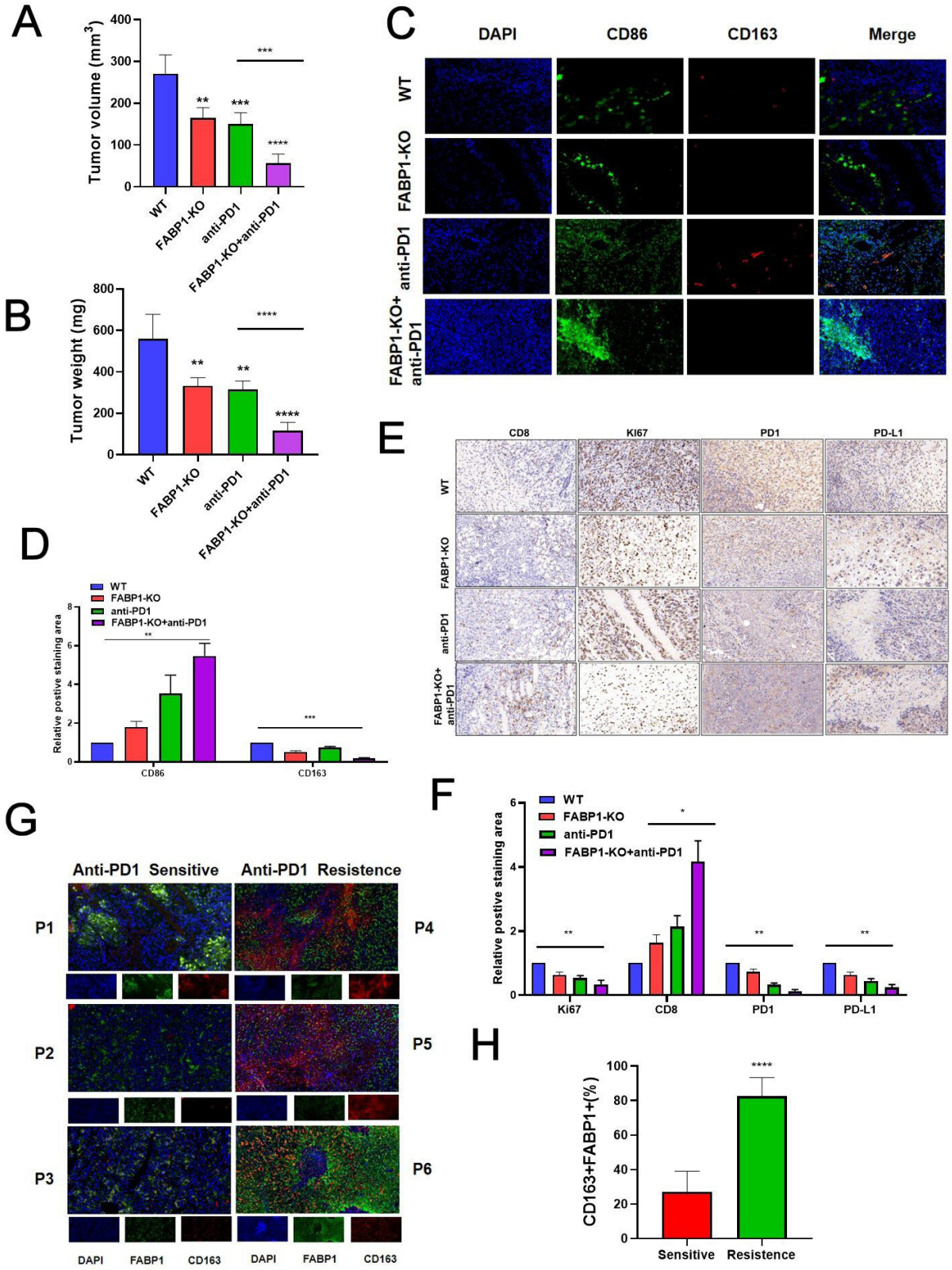

Figure 8 FABP1 deficiency enhanced sensitivity to anti-PD-1 therapy in hepatocellular carcinoma. (A) Analysis of tumor volume changes. (B) Analysis of tumor weight changes. (C–D) Immunofluorescence and analysis in different groups. (E–F) Immunohistochemical results and analysis in different groups. (G–H) Six non-responsive to anti-PD-1 treatment and five responsive to anti-PD-1 treatment human samples for immunofluorescence detection and analysis. Each row represents a patient, and the most representative images of three patients are displayed here. *p<0.05, **p<0.01, ***p<0.001,****p<0.0001. PD-1,programmed cell death 1; PD-L1, programmed cell death- ligand 1; KO, knockout; DAPI, 4',6-diamidino-2-phenylindole;FABP1, fatty acid binding protein 1; WT, wild type.

to anti-PD-1 treatment (anti-PD-1 non-responder group) and five puncture samples which responded to anti-PD-1 treatment (anti-PD-1 responder group), finding higher CD163+FABP1+ expression in anti-PD-1 non-responder group relative to responder group (figure 8G,H, online supplemental table S2). Therefore, FABP1 deficiency caused immune activation, meanwhile strengthening HCC cell sensitivity to anti-PD-1 therapy.

Orlistat as an FABP1 inhibitor restricted tumor growth and enhanced anti-PD-1 functions in HCC

Given that currently no drugs are capable of directly restricting FABP1, we adopted virtual screening for predicting small molecule compounds possibly inhibiting FABP1. We screened out 100 compounds, which can potentially bind to FBAP1. Online supplemental figure S20 displayed the first 20 compounds. According to the virtual screening results, orlistat is capable of binding to FABP1 and can potentially suppress cell functions (figure 9A). According to EdU, transwell, and scratch tests, TAMs in the orlistat group could remarkably weaken HCC cells (proliferation, invasion, and migration) relative to the control group (online supplemental figure S21). In vivo tests revealed that orlistat weakened the HCC tumor growth and the orlistat+anti-PD-1 group presented an obviously higher tumor inhibition rate relative to the phosphate-buffered saline (PBS)+anti-PD-1 group (figure 9G, online supplemental figure S22A,B). According to the findings of immunohistochemical analysis, orlistat caused a considerable reduction in the expression of Ki-67, PD-1, and PD-L1 while simultaneously enhancing the infiltration of CD8+T cells; this trend was made more apparent when combined with anti-PD-1 treatment (figure 9H, online supplemental figure S22C). The results of immunofluorescence showed that orlistat led to decreased expression of CD163 and increased expression of CD86 in tumor tissues. The combination of anti-PD-1 decreased this trend more pronounced (figure 9I,J).

Liposomes-loaded orlistat and IR780 probe weakened tumor growth and improved anti-PD-1 treatment efficiency in HCC

In order to improve more deeply the usage of orlistat and visualize the drug metabolism, we constructed a liposome as a carrier to encapsulate orlistat and fluorescence in liposome. The dynamic light scattering and zeta potentials of orlistat-coupled fluorescence on liposome were detected, and the zeta potential was 5.687 mV. Average particle size: 163.6 nm; intensity: 131.4 nm; Polymer dispersity index-(PDI): 0.3541 (figure 9B,C). Figure 9D,E showed the fluorescence imaging of liposome-loaded orlistat couples and liposome-loaded orlistat couples with IR780 probes, respectively. Standard and release curves for orlistat were shown in online supplemental figure S23A,B. After injection of liposome-loaded after the orlistat-IR780 probe was coupled to the tail vein of the mouse, we observed that the drug accumulated in the liver after 1 hour, and rarely accumulated in other organs for metabolism (figure 9F).

To investigate the relevance of liposome-loaded orlistat and IR780 probe to the antitumor effect of HCC in vivo, C57BL/6 mice was injected with H22 followed by anti-PD-1 in the liposome-loaded orlistat+IR780 probe group and the orlistat group, respectively. The liposome-loaded orlistat+IR780 probe significantly inhibited HCC growth, compared with the orlistat group. In addition, when anti-PD-1 was also administered, the liposome-loaded orlistat+IR780 probe group showed significantly higher inhibition of the tumor compared with the orlistat+anti-PD-1 group (figure 9G, online supplemental figure S22A,B). Immunohistochemical results showed that liposome-loaded orlistat+IR780 probe significantly decreased Ki-67, PD-1, PD-L1 expression than orlistat alone, and also significantly increased CD8+T-cell infiltration, with a more pronounced trend of combined anti-PD-1 (figure 9H, online supplemental figure S22C). Immunofluorescence results showed that the liposome-loaded orlistat+IR780 probe decreased CD163 and increased CD86 expression in tumor tissues more significantly than orlistat alone (figure 9I,J). Overall, liposome-loaded orlistat+IR780 probes reduced cancer growth and significantly improved the anti-PD-1 treatment efficacy for HCC.

FABP1 exhibited high enrichment in TAMs in metastatic HCC tissues

Since FABP1 can promote the progression of HCC, we wonder whether FABP1 can impact the metastatic liver cancer process. We analyzed an analysis on the single-cell RNA data found in GSE164522, which came from primary colorectal cancer (CRC) as well as liver metastases. The fact that FABP1 from the TAM-CXCL12 cell cluster was greatly concentrated in both malignant and adjacent tissues of metastatic lesions, but not significantly expressed in initial lesions and adjacent tissues, was a discovery that took us by surprize (online supplemental figure S24A,B). After the injection of MC38 cells into the spleens of C57BL/6 mice (n=4) and FABP1−/− mice (n=4), the association of FABP1 with liver metastasis of CRC in vivo was examined. After that, we counted the number of changes in liver metastases. Accordingly, there was obviously less liver metastasis in FABP1−/− mice relative to WT mice (online supplemental figure S24C). Therefore, FABP1 can serve as a therapeutic target for liver metastasis of CRC.

DISCUSSION

The tumor cell-immune cell interaction in the TME critically impacts cancer progression. Immune cells engage in a dynamic dialog with tumor cells to help shape the process. Previous study has made use of the exceptional multidimensional capabilities of scRNA-seq in order to delineate the complex landscapes and cell–cell interactions that are present in human HCCs. Qiming Zhang *et al* used two scRNA-seq technologies in order to construct transcriptomes of patients with HCC's CD45+ immune

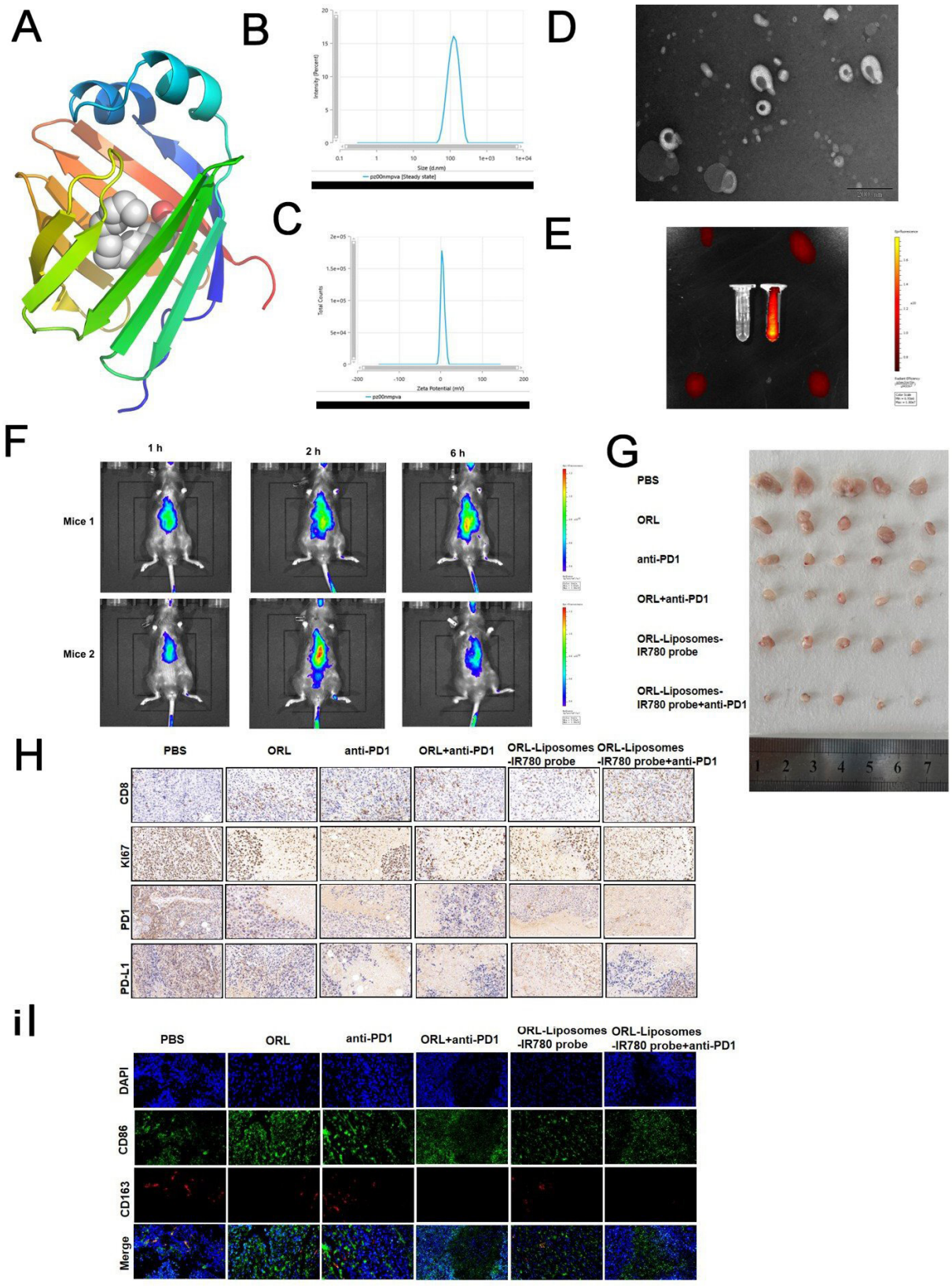

Figure 9 Orlistat as an FABP1 inhibitor reduced tumor growth and enhanced the effect of anti-PD-1 in hepatocellular carcinoma. (A) Map of the binding sites of orlistat and FABP1. (B) Dynamic light scattering potential of orlistat-coupled fluorescence on liposomes. (C) Zeta potential of orlistat-coupled fluorescence on liposomes. (D) Liposomes-loaded orlistat coupled fluorescence display. (E) Fluorescence imaging of liposomes loaded orlistat with IR780 probe. (F) Metabolic distribution of liposomes-loaded orlistat-linked IR780 probe in two mice. (G) Images of tumors in each group. (H) Immunohistochemical results in different groups. (I–J) Immunofluorescence and analysis in different groups. PD-1,programmed cell death 1;DAPI, 4',6-diamidino-2-phenylindole;ORL,Orlista; FABP1, fatty acid binding protein 1; PBS, phosphate-buffered saline.

cells from five immune-related sites. These sites were the tumor, the surrounding liver, the hepatic lymph node, the blood, and the ascites. The immune landscape of HCC was enriched with new aspects as a result of the dynamic features of various CD45+ cell types.[17] Yunfan Sun and colleagues analyzed the transcriptomes of 17,000 cells from 18 patients with different primary or early-relapse HCC. Two separate cohorts found that early-relapse tumors had lower Treg level, more DCs, and more CD8+T cells that had invaded the tumor, compared with initial tumors. Analysis of differential gene expression and interactions demonstrated the possible immune evasion mechanisms regarding recurring tumor cells. These mechanisms inhibit the antigen presentation by DC meanwhile recruiting innate-like CD8+T cells. Above findings helped to more deeply understand immune evasion mechanisms related to tumor relapse.[18] However, there is no study that investigates the variation in TME between the various stages of HCC. In the current study, deep scRNA-seq was conducted on immune cells in the isolation process in cancer tissues and adjacent respective tissues of three patients with HCC that were in the II-stage and four HCC cases that were in the III-stage. We discovered a variety of immune cell subtypes, including T/NK cells, B cells, and macrophages, and we characterized the developmental paths that each of these cell types follow. In addition, we investigated the enrichment pathways that each subtype uses. In particular, we went into greater detail regarding the TAMs found in the various samples. Our research offers a wealth of data as well as a theoretical foundation for the development of HCC.

It was interesting that FABP1 exhibited an overexpression in TAMs with III-stage HCC tissues, particularly in the metastatic foci, when compared with II-stage HCC tissues, and this conclusion was fully supported by immunofluorescence detection in more HCC human samples. Previous research has concentrated on the part that TAMs play in the progression of tumors. Using scRNA-seq, researchers found new hallmark genes of TAMs in lung adenocarcinoma.[19] These genes include triggering receptor with expressions on myeloid cells 2, macrophage receptor with collagenous structure, and apolipoprotein E. Besides, scRNA-seq of breast cancer showed that M2-type genes like CD163, membrane spanning 4-domains A6A, and transforming growth factor beta-1 (TGF-1) were expressed in TAMs. This was found in conjunction with the angiogenesis factors such as plasminogen activator, urokinase receptor, and interleukin (IL)-8.[20] These gene signature profiles found in TAMs showed relevance to patients' survival and contributed to new prospective targets for cancer treatment. TAMs reported a worse prognosis. Qiming Zhang *et al* confirmed the inflammatory functions exhibited by SLC40A1 and GPNMB and exhibited unique transcriptional states for TAMs and HCC.[17] The function and activity of FABP1 overexpression in TAMs to enhance HCC progression is the primary focus of our research for the first time. We also hope that future studies on cancer metastasis will focus on the function of TAMs.

The FABPs refer to a protein family consisting of no less than nine different members that are essential to the metabolism regarding fatty acids as well as other relevant molecules. It is believed that the level of FABP expression is in direct proportion to fatty acid metabolism rate.[21 22] FABPs all express themselves in a tissue-specific manner. In the liver, the metabolism involved as FABP1 partially affects long-chain fatty acid binding, transportation and metabolism.[23] Different from other FABP family members, the hydrophobic binding pocket in the center of FABP1 structure can bind to an especially broad spectrum regarding hydrophobic ligands meanwhile attaching various ligands.[24] Analysis of FABP1 expression by immunohistochemistry has the potential to be diagnostically useful due to the high tissue specificity of this technique. So far, studies that used FABP1 immunohistochemistry revealed that FABP1 was positive in 47–100% of HCC, 47.4–83.3% of lung cancer subtypes, 30–81.5% of colorectal carcinomas, 38.6% of gastric adenocarcinomas, 27–36.4% of kidney cancer subtypes, and 12.1% of pancreatic carcinomas.[25] Nevertheless, only a small number of studies have been done on its function in TME. Murai *et al* found that intratumoral lipid accumulation linked immune exhaustion to effective immune checkpoint inhibitors (ICI) therapy in non-viral HCC. Steatotic HCC accounts for 23% of non-viral HCC cases, presenting as immunoenriched but immunodepleted TME, characterized by T-cell failure, infiltration of M2 macrophages and cancer-related fibroblasts (CAF), high expression of PD-L1, and TGF-β signal activation. Spatial transcriptome analysis shows that M2 macrophages and CAFs may be very close to exhausted CD8+T cells in steatosis HCC.[26] Serum FABP1 levels are associated with low survival rates for chronic liver diseases ranging from chronic hepatitis to HCC.[27] FABP4 has been identified as a functional marker for protumor macrophages[28] and FABP4 upregulation contributes to the increased risk of breast cancer and non-viral and non-alcoholic HCC.[29] In addition, FABP5 expressed in CD8+cytotoxic lymphocytes(CTLs) has been shown to promote the uptake of linoleic acid, another long-chain fatty acid, and reactive oxygen species-mediated T-cell death, suggesting that FABP5 plays a role in mediating fatty acid-mediated immune failure in TME.[30] Therefore, Bing Li and Sauter made a comment that it is likely that FABPs function to mediate PD-1/PD-L1 upregulation in the TME, thus linking lipid accumulation to effective ICI therapy in HCC.[31]

In the present study, we found that the interaction between FABP1 and PPARG in TAMs facilitated the FAO promotion as well as the progression of HCC. According to previous reports, M1 and M2 macrophages generate their respective amounts of energy in very different ways. In contrast to M1 macrophages, which primarily use glycolysis for energy, M2 macrophages appear to favor oxidative phosphorylation, which they achieve through

boosting FAO.[32] In addition to this, it has been demonstrated that FAO inhibitor significantly reduces IL-4-induced activation of M2 macrophages.[33] This theory was, however, called into question by Namgaladze and Brüne, who showed that the FAO inhibitor had no discernible effect on human M2 macrophages after being treated to the cells.[34] Zhang *et al* revealed that the FAO inhibitor was able to suppress the protumoral impact brought about by a conditioned medium from M2-like TAMs on HCC. In addition, researchers more directly used several inhibitors against glutamine and glucose oxidation in addition to fatty acid production, which demonstrated that M2-like TAMs impacted HCC dependent on modulating FAO activity.[35] These same results were previously demonstrated to occur in HCC-associated macrophages when PPAR stimulation promoted M2-like polarization.[36] The findings of our study provide more evidence that TAMs can boost lipid metabolism and drive the growth of tumors.

One of the highlights of this study is that mass cytometry detects tumor samples from WT and FABP1−/− mice. Accordingly, Treg and NK cells showed a decreased relative proportion in FABP1−/− group relative to the WT group, whereas DC, M1 macrophages and B cells increased. In addition, it was revealed that the expression of PD-L1, PD-1, TIGIT, TIM-3, CTLA-4 decreased in FABP1−/− mice. It has been reported in the literature that in PD-1/PD-L1 treatment, tumors can block the antitumor effect of T cells by forming TME. This is possibly because antigen immunogenicity is inadequate, antigen presentation is dysfunctional, T-cell exhaustion is irreversible, cells resist interferon-γ signaling, and immunosuppression exists.[37] Therefore, reducing inhibitory immune cells is beneficial to enhance the effect of anti-PD-1. According to our finding, FABP1 deficiency caused immune activation of HCC. However, our research has some shortcomings here, such as not using FABP1 myeloid knockout mice. To further analyze the significance of whether FABP1 participating in the anti-PD-1 therapy resistant in human HCC tissues, we conducted immunofluorescence detection on six puncture samples in anti-PD-1 non-responder group and five puncture samples in anti-PD-1 responder group, finding higher CD163+FABP1+ expression in the former than the latter. Our findings provide a marker and a target for the sensitivity of anti-PD-1 treatment in HCC.

In order to transform our research results as soon as possible, we screened small molecular libraries and found orlistat significantly inhibited FABP1 activity, while the combination of anti-PD-1 could synergistically treat HCC progression. Liposomes loaded with orlistat and connected with IR780 probe could further enhance the therapeutic effect of orlistat and visualize drug metabolism in vivo. Zhang Cong *et al* revealed the antilipogenic and antiproliferative actions exhibited by orlistat in hepatocarcinogenesis, providing its benefits for treating HCC.[38] Orlistat also can resist tumor and strengthen paclitaxel efficacy in Hep3B cells.[33] In addition, orlistat modulates metabolism to make HCC cells resensitive to sorafenib.[39] Our study provides a new indication for orlistat and brings new hope and benefits to patients with advanced HCC.

It is worth mentioning that we also analyzed single-cell RNA data from primary and liver metastasis from CRC. We were surprised to find that FABP1 from the TAM-CXCL12 cell cluster was highly enriched in both cancerous and adjacent tissues of metastatic lesions, but not significantly expressed in primary lesions and adjacent tissues. According to in vivo results, there is less liver metastasis in FABP1−/− mice relative to WT mice. In our earlier study, Matrix Gla protein(MGP) activated the nuclear factor kappa-B(NF-κB) pathway to accelerate CD8+T-cell exhaustion, which ultimately caused liver metastasis of CRC. It is allowed to achieve synergistic resistance to liver metastasis of CRC when MGP knockdown is combined with anti-PD-1 combination.[40] In this study, our research group discovered a gene-FABP1 for the first time that promotes liver metastasis of CRC in macrophages. Macrophages are changeable cells that, depending on the surrounding microenvironment, can either become tumor-killing macrophages or protumorigenic macrophages. Through the production of CCL2, tumor cells in liver metastases were able to recruit monocytes and TAMs from the host's liver. Additionally, adoptive transfer of inflammatory monocytes resulted in preferential migration to metastatic sites and the subsequent differentiation of those monocytes into macrophages.[41] Through the process of producing liver fibrosis and immunosuppression, the recruitment of macrophages in the liver enhanced the process of liver metastasis.[42] Both CCR2 antagonists and the deletion of CCL2 in tumor cells caused obviously weakened metastatic cancer burden.[43–45] Ndrg2 gene loss in macrophages led to a shift in polarization of TAMs toward an M1 phenotype in a mouse model of CRC liver metastasis.[46] That resulted in a reduction in the severity of CRC liver metastasis. Researchers Yingcheng Wu and colleagues observed that metastatic cancers include an abundance of immune-suppressive cells, particularly MRC1+CCL18+ M2like macrophages.[47] Through scRNA-seq, as well as in vitro and in vivo investigations, we thoroughly clarified the function and mechanism of FABP1 in TAMs. This led to the discovery of new targets and therapeutic possibilities for primary and secondary liver cancer.

There are some limitations to our article. Although our article found the cancer-promoting effect of FABP1 in HCC and the potential therapeutic value of targeting FABP1, some more in-depth mechanisms need to be further studied due to funding lacking present and other reasons. We found that FABP1 expression was significantly higher in cancerous tissues, MVI, and thrombus than in para-cancerous tissues, and FABP1 expression was higher in stage III tumors than in stage II tumors. Although we verified through a series of experiments that the tumor supernatant could induce the increase of FABP1 in TAM and thus lead to the increase of M2 polarization, we did not further explore which factors in

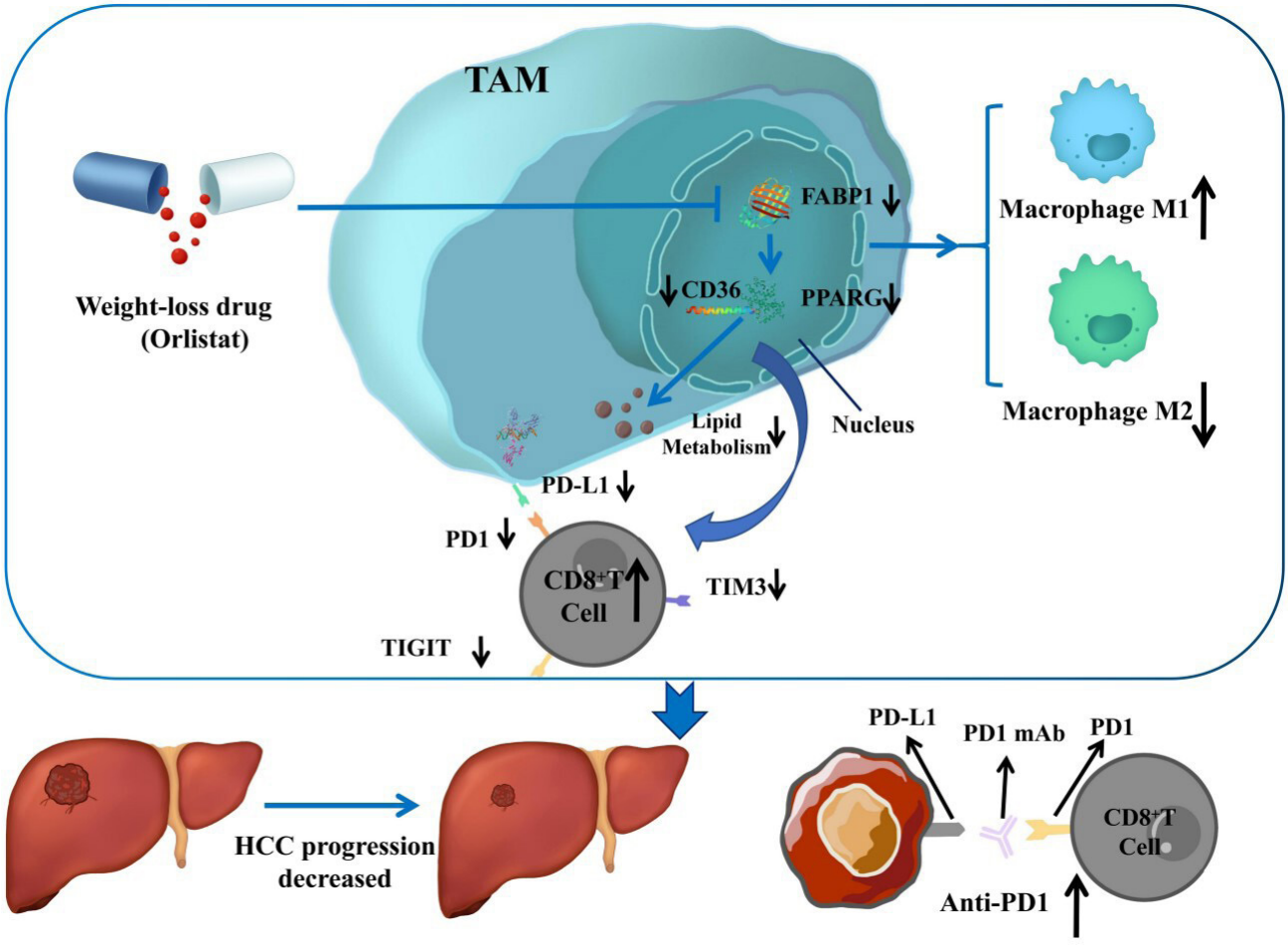

Figure 10 Pattern diagram showing that inhibition of FABP1 in TAMs inhibited HCC progression in vitro and in vivo . Moreover, FABP1 interacted with PPARG in TAMs to promote lipid metabolism and progress of HCC. In further clinical translation, we found that orlistat significantly inhibited FABP1 activity, while the combination of anti-PD-1 could synergistically treat HCC progression. FABP1, fatty acid binding protein 1; HCC, hepatocellular carcinoma; TAMs, tumor-associated macrophages.

the tumor supernatant induced the increase of FABP1. In addition, though the above phenomenon we found has been verified by a series of cell experiments and the construction of subcutaneous implantation models of transplanted tumors and knockout mouse models, MVI mouse models cannot be established at present, which may not fully prove the mechanism of FABP1 elevation in MVI to a certain extent. We will continue to explore the above defects in the subsequent research.

In conclusion, FABP1 was overexpressed in TAMs with III-stage HCC tissues relative to II-stage HCC tissues, and such conclusion was fully confirmed by immunofluorescence detection in more HCC human samples. Inhibition of FABP1 in TAMs restricted HCC progression in vitro and in vivo. Moreover, FABP1 interacted with PPARG in TAMs to promote FAO and progress of HCC. We found in further clinical practise that orlistat significantly inhibited FABP1 activity, while the combination of anti-PD-1 could synergistically treat HCC progression (figure 10). Liposomes loaded with orlistat and connected with IR780 probe could further enhance the therapeutic effect of orlistat and visualize drug metabolism in vivo.

MATERIALS AND METHODS

Ethics statement

Regarding the application of samples to experiments, the respective case supplied written consent for informed consent. In addition, this study followed all applicable guidelines and regulations.

Patients and specimens

Deep scRNA-seq was conducted on immune cells isolated in cancer tissues and adjacent respective tissues of 3 II-stage and 4 III-stage HCC cases. We obtained six samples (three pairs of tissues) from GSA: HRA000069 and EGA: EGAS00001003449 for patients with 3 II-stage HCC. This HCC data analysis is also available at http://cancer-pku.cn:3838/HCC/. Hepatobiliary/Liver Transplantation Center, the First Affiliated Hospital of Nanjing Medical University, provided four instances of stage III HCC and nine samples (online supplemental table S3). The pathologist diagnoses the sample location's pathology.

Gene Expression Omnibus(GEO) accession number GSE164522 contains the processed gene expression data of liver metastasis from CRC in this study. It is allowed

to analyze and visualize scRNA-seq data sets at http://cancer-pku.cn:3838/CRLM/. Due to patient privacy concerns, the raw FASTQ files from the study will be made available for scientific research on law request. On request, the source code for all the processing and analysis can be accessible.

For the patient information related to immunofluorescence mentioned in the article, please refer to online supplemental tables S1 and S2 for details.

scRNA-seq analysis

The scRNA-seq analysis was described in detail in the previous article.[48] The number of cells in each sample is detailed in the online supplemental table S3.

Cancer cell culture

The Cell Bank of Type Culture Collection provided mice H22-HCC cells and human HCC cells (YY8103 and HCCLM3), cultured in Roswell Park Memorial Institute(RPMI) 1640 medium with 10% fetal bovine serum(FBS) at 37°C in a 5% CO_2 chamber. We maintained cell lines in an incubator (5% CO_2) and a constant temperature of 37°C.

THP-1 primary culture and cell transfection

THP-1 cells underwent culture in 5% CO_2 at 37°C in RPMI 1640 media added with 10% FBS and siRNA (GeneChem, China) was transfected into cells. After 2 days of Phorbol-12-myristate-13-acetate-induced macrophage differentiation, THP-1 cells were collected, which was named M0 macrophages. In TAM stimulation tests, M0 macrophage cells received the treatment of YY8103/HCCLM3 cell culture supernatant in RPMI 1640 media for 3 days, which resulted in the production of what are known as TAMs. Details were described in the previous article.[49]

Cell proliferation assay

YY8103 and HCCLM3 cells were treated with 50% conditioned medium obtained from TAMs treated with si-NC or si-FABP1 for the EdU test. Details were described in the previous article.[49]

Transwell assay

The cells YY8103 and HCCLM3 were treated with 50% conditioned medium obtained from TAMs treated with si-NC or si-FABP1. RPMI 1640 medium free of serum were used to seed YY8103 and HCCLM3 cells in upper chambers. Details were described in the previous article.[49]

Scratch wound experiment

When the cell fusion reached about 90% 48 hours after transfection, the tip of pipette was used to create a wound, and culture medium was used to flush the cells to remove free floating cells and debris. Details were described in the previous article.[49] qRT-PCR as per the protocol of the manufacturer, total RNAs were isolated from TAMs using TRIzol reagent (Invitrogen, USA). Reverse transcription kit (Takara, Japan) assisted in synthesizing complementary DNA into messenger RNA (mRNA). Glyceraldehyde-3-phosphate dehydrogenase(GAPDH) assisted in standardizing mRNA expression level. The sequences of all primers are provided in online supplemental table S4.

Immunofluorescence and immunohistochemistry

Immunofluorescent cells underwent 20 min of fixation by using 4% paraformaldehyde at room temperature and 5 min of permeabilization of 0.05% Triton X-100 in PBS. Samples underwent one night of blocking in PBS 2% Albumin from bovine serum(BSA) and the incubation of antibodies specific to CD163 and FABP1 at 4°C before being conjugated with Alexa Fluorite or Horseradish Peroxidase(HRP).

Sections with a paraffin embedding were deparaffinized and rehydrated for immunohistochemistry. Hydrogen peroxide inhibited the activity of peroxidase. Sections underwent one night of incubation by a primary antibody cocktail (PD-1, CD8, Ki67, PD-1, and PD-L1, Abcam, UK) at 4°C.

Western blotting and co-immunoprecipitation

Radio-Immunoprecipitation Assay(RIPA) buffer solution was employed for isolating proteins from cells. The isolated proteins received lysis of Sodium dodecyl sulfate(SDS)-polyacrylamide gels, and then were transferred to the Polyvinylidenefluoride(PVDF) membranes. Using primary antibodies against FABP1, PPARG, CD36, and PD-L1 (Abcam, UK), the control group was given with GAPDH. Using enhanced chemiluminescence, a peroxidase-conjugated secondary antibody (CST, Sigma-Aldrich, USA) was employed.

The 293T cells were planted for 24 hours in 6-well tissue culture plates and cotransfected with the plasmids. The supernatants were incubated with anti-HA or anti-FLAG magnetic beads (Bimake, Texas, USA), washed three times, and then incubated overnight at 4°C. Details were described in the previous article.[49]

Nile red assay

Cells from various groups were stained with Nile red 24 hours later (Solarbio Life Sciences, China). According to the manufacturer's directions, staining was done. An inverted fluorescent microscope (Nikon, Japan) was used to capture the photographs.

Virtual screening

The Molecular Operating Environment(MOE) dock module was used for structure-based virtual screening(VS). As a vs library, the authorized drug molecules in DrugBank were selected. All compounds were created using the MOE Wash module. The structure of FABP1 predicted by AlphaFold was defined as a receptor. The Site Finder module in MOE was used to define the binding site. Then, we ranked all compounds with the flexible docking protocol "induced fit". Specific to flexible docking, we first ranked the docked poses based on the London dG score, then refined the force field on the top 10 poses, and rescored GBVI/WSA dG, meanwhile

keeping pose with the highest rank. The top 100 ranked molecules were recognized as possible hits.

Construction of liposomes loaded with orlistat IR780 probe

Phospholipids 70 mg, DSPE-PEG-NH3 10 mg, cholesterol 15 mg, and orlistat 10 mg were dissolved in 5 mL chloroform, and then ultrasonic dissolved for 3 min. The solution was added to an eggplant shaped bottle and connected to a rotating evaporator. The eggplant shaped bottle was removed and placed at room temperature. 8 mL of fluorescent water was added and the rotary evaporator was reconnected. 10 mg of liposome was added to 100 mM PBS buffer solution, 5 mg of N-(3-Dimethylaminopropyl)-N'-ethylcarbodiimide hydrochloride(EDC) and 2 mg of fluorescence were added, and stirred overnight.

Mice model

The animal experiment has obtained the approval of the animal management committee of Nanjing Medical University (2021-SRFA-197). All experiment techniques and animal care complied with the institution's ethical guidelines for animal experimental operations. The H22 cells were injected into mice (n=5 in each group). We divided tumor model mice transplanted with carcinoma into four groups, each containing five mice: the WT group, the FABP1−/− group, the anti-PD-1 group, and the FABP1−/− + anti-PD-1 group. These groups received treatments that corresponded to their respective groups. Anti-PD-1 or FABP1−/− + anti-PD-1 group was intraperitoneally injected with 6.6 mg/kg on the eighth day, followed by injections two times a week.

Experiment with WT mice (orlistat): H22 cells were injected into C57BL/6 mice. Mice with implanted cancerous tumors were divided into six groups, each with five mice: PBS, orlistat, anti-PD-1, orlistat+anti-PD-1, orlistat-liposomes+IR780 probe, and orlistat-liposomes+IR780 probe+anti-PD-1. Specifically, orlistat was injected intraperitoneally with 5 mg/kg on the first day and one time every 4 days thereafter; anti-PD-1 was administered intraperitoneally with 6.6 mg/kg on the eighth day and two times a week thereafter.

Mass cytometry

We obtained the tissue samples respectively from tumors of FABP1−/− and WT C57BL/6 mice. The analysis were described in detail in the previous article.[49]

Statistical analysis

GraphPad Prism V.8.0 served for statistical analysis. P value<0.05 reported statistical significance. An independent t-test compared continuous variables between two groups. A one-way analysis of variance compared continuous variables between multiple groups.

Author affiliations
[1]Hepatobiliary/Liver Transplantation Center, The First Affiliated Hospital of Nanjing Medical University, Key Laboratory of Living Donor Transplantation, Chinese Academy of Medical Sciences, Nanjing, Jiangsu, China
[2]Nanjing Medical University, Nanjing, Jiangsu, China
[3]Jiangsu Key Laboratory of Infection and Immunity, Institute of Biology and Medical Sciences, Soochow University, Suzhou, Jiangsu, China
[4]First Teaching Hospital of Tianjin University of Traditional Chinese Medicine, Tianjin University of Traditional Chinese Medicine, Tianjin, China

Contributors Four first authors made equal contribution to the project. XW is responsible for the overall content as the guarantor.WT, GS, G-WJ and TF took charge of the collection of HCC tissue specimen as well as adjacent non-tumorous tissues, and manuscript drafting. WT and GS designed and performed experiments. QZ, HC, WW, XZ, CL, HL and TH performed part of the experiments, as well as interpreted data. Besides, there were three corresponding authors. LL took charge of data interpretation. XW, YX and LL designed the study and critically revised manuscript. The final manuscript has been read by and obtained the approval of all authors.

Funding This work was completed with the support from the National Natural Science Key Foundation of China (Grant No.31930020).

Competing interests No, there are no competing interests.

Patient consent for publication Not applicable.

Ethics approval Ethical review unit: The First Affiliated Hospital of Nanjing Medical University (Jiangsu Provincial People's Hospital). Ethical approval number: 2019-SRFA-238. Participants gave informed consent to participate in the study before taking part.

Provenance and peer review Not commissioned; externally peer reviewed.

Data availability statement Data are available upon reasonable request.

ORCID iDs
Weiwei Tang http://orcid.org/0000-0002-8516-819X
Gu-Wei Ji http://orcid.org/0000-0003-1736-062X
Yongxiang Xia http://orcid.org/0000-0001-6589-797X

REFERENCES

1 Omata M, Cheng A-L, Kokudo N, *et al*. Asia-Pacific clinical practice guidelines on the management of hepatocellular carcinoma: a 2017 update. *Hepatol Int* 2017;11:317–70.
2 Marrero JA, Kulik LM, Sirlin CB, *et al*. Diagnosis, staging, and management of hepatocellular carcinoma: 2018 practice guidance by the American Association for the study of liver diseases. *Hepatology* 2018;68:723–50.
3 European Association for the Study of the Liver. Electronic address eee, European Association for the Study of the L. EASL clinical practice guidelines: management of hepatocellular carcinoma. *J Hepatol* 2018;69:182–236.
4 Petrick JL, Kelly SP, Altekruse SF, *et al*. Future of hepatocellular carcinoma incidence in the United States forecast through 2030. *J Clin Oncol* 2016;34:1787–94.
5 Kee K-M, Wang J-H, Lee C-M, *et al*. Validation of clinical AJCC/UICC TNM staging system for hepatocellular carcinoma: analysis of 5,613 cases from a medical center in Southern Taiwan. *Int J Cancer* 2007;120:2650–5.
6 Llovet JM, Brú C, Bruix J. Prognosis of hepatocellular carcinoma: the BCLC staging classification. *Semin Liver Dis* 1999;19:329–38.
7 Bridges K, Miller-Jensen K. Mapping and validation of scRNA-Seq-derived cell-cell communication networks in the tumor Microenvironment. *Front Immunol* 2022;13:885267.

8 Li Y, Jin J, Bai F. Cancer biology deciphered by single-cell Transcriptomic sequencing. *Protein Cell* 2022;13:167–79.
9 González-Silva L, Quevedo L, Varela I. Tumor functional heterogeneity unraveled by scRNA-Seq Technologies. *Trends Cancer* 2020;6:13–9.
10 Yang KR, Mooney SM, Zarif JC, *et al*. Niche inheritance: a cooperative pathway to enhance cancer cell fitness through Ecosystem engineering. *J Cell Biochem* 2014;115:1478–85.
11 Piñeiro Fernández J, Luddy KA, Harmon C, *et al*. Hepatic tumor Microenvironments and effects on NK cell phenotype and function. *Int J Mol Sci* 2019;20:4131.
12 Wang Y, Jia M, Liang C, *et al*. Anterior gradient 2 increases long-chain fatty acid uptake via stabilizing Fabp1 and facilitates lipid accumulation. *Int J Biol Sci* 2021;17:834–47.
13 Rodriguez Sawicki L, Bottasso Arias NM, Scaglia N, *et al*. Fabp1 knockdown in human Enterocytes impairs proliferation and alters lipid metabolism. *Biochim Biophys Acta Mol Cell Biol Lipids* 2017;1862:1587–94.
14 Valizadeh M, Aghasizadeh M, Nemati M, *et al*. The association between a fatty acid binding protein 1 (Fabp1) gene polymorphism and serum lipid abnormalities in the MASHAD cohort study. *Prostaglandins Leukot Essent Fatty Acids* 2021;172:S0952-3278(21)00086-7.
15 Su P, Wang Q, Bi E, *et al*. Enhanced lipid accumulation and metabolism are required for the differentiation and activation of tumor-associated Macrophages. *Cancer Res* 2020;80:1438–50.
16 Liu S, Zhang H, Li Y, *et al*. S100A4 enhances Protumor macrophage polarization by control of PPAR-gamma-dependent induction of fatty acid oxidation. *J Immunother Cancer* 2021;9:e002548.
17 Zhang Q, He Y, Luo N, *et al*. Landscape and Dynamics of single immune cells in hepatocellular carcinoma. *Cell* 2019;179:829–845.
18 Sun Y, Wu L, Zhong Y, *et al*. Single-cell landscape of the Ecosystem in early-relapse hepatocellular carcinoma. *Cell* 2021;184:404–421.
19 Lavin Y, Kobayashi S, Leader A, *et al*. Innate immune landscape in early lung adenocarcinoma by paired single-cell analyses. *Cell* 2017;169:750–65.
20 Chung W, Eum HH, Lee H-O, *et al*. Single-cell RNA-Seq enables comprehensive tumour and immune cell profiling in primary breast cancer. *Nat Commun* 2017;8:15081.
21 Smathers RL, Petersen DR. The human fatty acid-binding protein family: evolutionary Divergences and functions. *Hum Genomics* 2011;5:170–91.
22 Thumser AE, Moore JB, Plant NJ. Fatty acid binding proteins: tissue-specific functions in health and disease. *Curr Opin Clin Nutr Metab Care* 2014;17:124–9.
23 Vergani L, Fanin M, Martinuzzi A, *et al*. Liver fatty acid-binding protein in two cases of human lipid storage. *Mol Cell Biochem* 1990;98:225–30.
24 Furuhashi M, Hotamisligil GS. Fatty acid-binding proteins: role in metabolic diseases and potential as drug targets. *Nat Rev Drug Discov* 2008;7:489–503.
25 Dum D, Ocokoljic A, Lennartz M, *et al*. Fabp1 expression in human tumors: a tissue Microarray study on 17,071 tumors. *Virchows Arch* 2022;481:945–61.
26 Murai H, Kodama T, Maesaka K, *et al*. Multiomics identifies the link between Intratumor steatosis and the exhausted tumor immune Microenvironment in hepatocellular carcinoma. *Hepatology* 2023;77:77–91.
27 Eguchi A, Hasegawa H, Iwasa M, *et al*. Serum liver-type fatty acid-binding protein is a possible Prognostic factor in human chronic liver diseases from chronic hepatitis to liver cirrhosis and hepatocellular carcinoma. *Hepatol Commun* 2019;3:825–37.
28 Hao J, Yan F, Zhang Y, *et al*. Expression of Adipocyte/macrophage fatty acid-binding protein in tumor-associated Macrophages promotes breast cancer progression. *Cancer Res* 2018;78:2343–55.
29 Chiyonobu N, Shimada S, Akiyama Y, *et al*. Fatty acid binding protein 4 (Fabp4) overexpression in Intratumoral hepatic Stellate cells within hepatocellular carcinoma with metabolic risk factors. *Am J Pathol* 2018;188:1213–24.
30 Jin R, Hao J, Yi Y, *et al*. Dietary fats high in Linoleic acids impair antitumor T-cell responses by inducing E-FABP-mediated mitochondrial dysfunction. *Cancer Res* 2021;81:5296–310.
31 Li B, Sauter ER. Lipids link immune suppression to effective Immunotherapy in Steatotic hepatocellular carcinoma. *Ann Transl Med* 2023;11:226.
32 Kelly B, O'Neill LAJ. Metabolic Reprogramming in Macrophages and Dendritic cells in innate immunity. *Cell Res* 2015;25:771–84.
33 Huang SC-C, Everts B, Ivanova Y, *et al*. Cell-intrinsic lysosomal Lipolysis is essential for alternative activation of Macrophages. *Nat Immunol* 2014;15:846–55.
34 Namgaladze D, Brüne B. Fatty acid oxidation is Dispensable for human macrophage IL-4-induced polarization. *Biochim Biophys Acta* 2014;1841:1329–35.
35 Zhang Q, Wang H, Mao C, *et al*. Fatty acid oxidation contributes to IL-1β secretion in M2 Macrophages and promotes macrophage-mediated tumor cell migration. *Mol Immunol* 2018;94:27–35.
36 Wu L, Zhang X, Zheng L, *et al*. Ripk3 Orchestrates fatty acid metabolism in tumor-associated Macrophages and Hepatocarcinogenesis. *Cancer Immunol Res* 2020;8:710–21.
37 Lei Q, Wang D, Sun K, *et al*. Resistance mechanisms of anti-Pd1/Pdl1 therapy in solid tumors. *Front Cell Dev Biol* 2020;8:672.
38 Zhang C, Sheng L, Yuan M, *et al*. Orlistat delays Hepatocarcinogenesis in mice with hepatic Co-activation of AKT and C-met. *Toxicol Appl Pharmacol* 2020;392:S0041-008X(20)30042-9.
39 You BJ, Chen LY, Hsu PH, *et al*. Orlistat displays antitumor activity and enhances the efficacy of paclitaxel in human hepatoma Hep3B cells. *Chem Res Toxicol* 2019;32:255–64.
40 Shueng PW, Chan HW, Lin WC, *et al*. Orlistat Resensitizes sorafenib-resistance in hepatocellular carcinoma cells through Modulating metabolism. *Int J Mol Sci* 2022;23:6501.
41 Rong D, Sun G, Zheng Z, *et al*. MGP promotes Cd8(+) T cell exhaustion by activating the NF-kappaB pathway leading to liver metastasis of colorectal cancer. *Int J Biol Sci* 2022;18:2345–61.
42 Qian B-Z, Li J, Zhang H, *et al*. Ccl2 recruits inflammatory monocytes to facilitate breast-tumour metastasis. *Nature* 2011;475:222–5.
43 Nielsen SR, Quaranta V, Linford A, *et al*. Macrophage-secreted Granulin supports Pancreatic cancer metastasis by inducing liver fibrosis. *Nat Cell Biol* 2016;18:549–60.
44 Mitchem JB, Brennan DJ, Knolhoff BL, *et al*. Targeting tumor-infiltrating Macrophages decreases tumor-initiating cells, relieves immunosuppression, and improves chemotherapeutic responses. *Cancer Res* 2013;73:1128–41.
45 Zhao L, Lim SY, Gordon-Weeks AN, *et al*. Recruitment of a myeloid cell subset (Cd11B/Gr1 mid) via Ccl2/Ccr2 promotes the development of colorectal cancer liver metastasis. *Hepatology* 2013;57:829–39.
46 Li M, Lai X, Zhao Y, *et al*. Loss of Ndrg2 in liver Microenvironment inhibits cancer liver metastasis by regulating tumor associate Macrophages polarization. *Cell Death Dis* 2018;9:248.
47 Wu Y, Yang S, Ma J, *et al*. Spatiotemporal immune landscape of colorectal cancer liver metastasis at single-cell level. *Cancer Discov* 2022;12:134–53.
48 Hao X, Zheng Z, Liu H, *et al*. Inhibition of Apoc1 promotes the transformation of M2 into M1 Macrophages via the Ferroptosis pathway and enhances anti-Pd1 Immunotherapy in hepatocellular carcinoma based on single-cell RNA sequencing. *Redox Biol* 2022;56:102463.
49 Sun G, Liu H, Zhao J, *et al*. Macrophage Gsk3Beta-deficiency inhibits the progression of hepatocellular carcinoma and enhances the sensitivity of anti-Pd1 Immunotherapy. *J Immunother Cancer* 2022;10:e005655.